A Musculoskeletal Model of the Equine Forelimb for Determining Surface Stresses and Strains in the Humerus—Part II. Experimental Testing and Model Validation

Sarah Pollock
Biomedical Engineering Program,
University of California,
One Shields Avenue,
Davis, CA 95616

Susan M. Stover
Department of Anatomy, Physiology and Cell Biology,
School of Veterinary Medicine,
and Biomedical Engineering Program,
University of California,
One Shields Avenue,
Davis, CA 95616

M. L. Hull[1]
Department of Mechanical Engineering,
and Biomedical Engineering Program,
University of California,
One Shields Avenue,
Davis, CA 95616
e-mail: mlhull@ucdavis.com

Larry D. Galuppo
Department of Anatomy, Physiology, and Cell Biology,
School of Veterinary Medicine,
University of California,
One Shields Avenue,
Davis, CA 95616

*The first objective of this study was to experimentally determine surface bone strain magnitudes and directions at the donor site for bone grafts, the site predisposed to stress fracture, the medial and cranial aspects of the transverse cross section corresponding to the stress fracture site, and the middle of the diaphysis of the humerus of a simplified in vitro laboratory preparation. The second objective was to determine whether computing strains solely in the direction of the longitudinal axis of the humerus in the mathematical model was inherently limited by comparing the strains measured along the longitudinal axis of the bone to the principal strain magnitudes and directions. The final objective was to determine whether the mathematical model formulated in Part I [Pollock et al., 2008, ASME J. Biomech. Eng., **130**, p. 041006] is valid for determining the bone surface strains at the various locations on the humerus where experimentally measured longitudinal strains are comparable to principal strains. Triple rosette strain gauges were applied at four locations circumferentially on each of two cross sections of interest using a simplified in vitro laboratory preparation. The muscles included the biceps brachii muscle in addition to loaded shoulder muscles that were predicted active by the mathematical model. Strains from the middle grid of each rosette, aligned along the longitudinal axis of the humerus, were compared with calculated principal strain magnitudes and directions. The results indicated that calculating strains solely in the direction of the longitudinal axis is appropriate at six of eight locations. At the cranial and medial aspects of the middle of the diaphysis, the average minimum principal strain was not comparable to the average experimental longitudinal strain. Further analysis at the remaining six locations indicated that the mathematical model formulated in Part I predicts strains within ±2 standard deviations of experimental strains at four of these locations and predicts negligible strains at the remaining two locations, which is consistent with experimental strains. Experimentally determined longitudinal strains at the middle of the diaphysis of the humerus indicate that tensile strains occur at the cranial aspect and compressive strains occur at the caudal aspect while the horse is standing, which is useful for fracture fixation.* [DOI: 10.1115/1.2898729]

Introduction

A musculoskeletal mathematical model for computing the stresses and strains that occur in the proximal half of the equine humerus created by the surrounding musculature and ground reaction forces while standing was described in [1] (hereafter referred to as Part I of this two-part article). Analyses using this model provided the strains that occur on the lateral, medial, caudal, and cranial aspects of the transverse cross sections of the humerus corresponding to the donor site for bone grafts, a site predisposed to stress fracture, and the middle of the diaphysis. Knowing the strains that occur at the site of the proximocaudal humerus that is predisposed to stress fractures is important for injury treatment and fracture prevention [2]. Identifying the strains at the site of the humerus proposed for harvest of autogenous bone graft material is necessary for evaluating the feasibility of obtaining donor bone from this location [3]. Knowing the specific regions of the middle of the diaphysis that experience tensile and compressive strains would assist in determining optimum placement of internal fixation devices for the treatment of complete fractures [2].

To make the mathematical model tractable, modeling assumptions were made. Both equine [4] and canine [5] EMG data for forelimb muscles during the stance phase of walking were used to determine which specific shoulder muscles to include in the mathematical model. To allocate forces to active shoulder muscles, constrained optimization was used to minimize the sum of the cubed muscle stress, which is thought to maximize muscular endurance [6]. To calculate surface stresses for the cortical bone shell of the humerus from predicted shoulder muscle forces, the mathematical method of asymmetrical beam analysis was used [7,8]. The effects of torsion and shear forces were not considered, resulting in stresses and strains calculated only in the direction on

[1]Corresponding author.

Contributed by the Bioengineering Division of ASME for publication in the JOURNAL OF BIOMECHANICAL ENGINEERING. Manuscript received May 10, 2006; final manuscript received July 10, 2007; published online May 29, 2008. Review conducted by Andrew A. Amis.

the longitudinal axis of the humerus. Therefore, it is important to validate the mathematical model due to the various assumptions upon which the model is based.

This paper describes the experimental methods used to test an equine preparation and validate the strains calculated with the musculoskeletal mathematical model. The first objective was to experimentally determine surface bone strain magnitudes and directions at the specific bone graft donor site, and the cross sections on the humerus corresponding to the site predisposed to stress fracture and the middle of the diaphysis. The second objective was to determine whether computing strains solely in the direction of the longitudinal axis of the humerus in the mathematical model was inherently limited by comparing the strains measured along the longitudinal axis of the bone to the principal strain magnitudes and directions. The final objective was to determine whether the mathematical model formulated in Part I is valid for determining the surface strains at the various locations on the humerus where experimentally measured longitudinal strains correlate to principal strains.

Methods

Simplified In Vitro Musculoskeletal Preparation. One forelimb from each of eight horses (two Thoroughbred, four Quarter horses, one Swedish warmblood, and one Missouri Foxtrotter; ages 2–14 years) was wrapped in saline-soaked towels, frozen, and thawed before dissection and testing. Each limb was transversely sectioned at the level of the middle of the radius and all skin, fascia, and muscles were removed except for the supraspinatus, infraspinatus, subscapularis, and biceps brachii muscle-tendon unit. Therefore, the simplified preparation consisted of the scapula, humerus, proximal half of the radius and ulna (antebrachium), the biceps brachii muscle to provide the contact force on the proximocranial aspect of the humerus, and other muscles that were predicted to be active during stance by the optimization procedure.

The antebrachium was fixed to the actuator of a materials testing machine (MTS Systems Corp., Minneapolis, MN) using polymethylmethacrylate (COE Tray, GC America Inc., Alsip, IL). The scapula was secured to a load cell (at 2/3 the length of the scapula, measured from the glenoid cavity along the length of the scapular spine) by a fixture that allowed for scapular rotation in the sagittal plane, and thus changes in shoulder and elbow joint angles during loading. Shoulder and elbow angles were confirmed (100 deg and 135 deg, respectively) at a test load of 1335 N, which is equivalent to a standing vertical ground reaction load based on a forelimb supporting 30% of the entire weight of the horse while standing [9].

To replicate the forces of the shoulder muscles as predicted active by the mathematical model, the infraspinatus, subscapularis, and both lateral and medial heads of the supraspinatus were completely transected proximal to their tendinous insertion on the humerus. A load was then applied to each transected muscle via a weight to simulate active force production as predicted with optimization. A clamp was attached to the tendon of the transected muscle near the humerus, a cable was run along the line of action of the muscle from each clamp through a pulley system, and weights were hung from the cable that corresponded to the predicted active load of the muscle (lateral supraspinatus=57 N, medial supraspinatus=41 N, infraspinatus=74 N, and subscapularis =320 N) (Fig. 1).

Experimentally Determined Strains. Strain gauges were applied to the stress fracture site (caudal), medial and cranial aspects of the transverse cross section corresponding to the stress fracture site, the bone graft donor site (lateral) corresponding to the bone graft donor cross section, and to the lateral, caudal, medial, and cranial aspects of the mid-diaphyseal transverse cross section of the humerus. Due to the proximity of the bone graft donor and stress fracture cross sections on the proximal humerus, and to

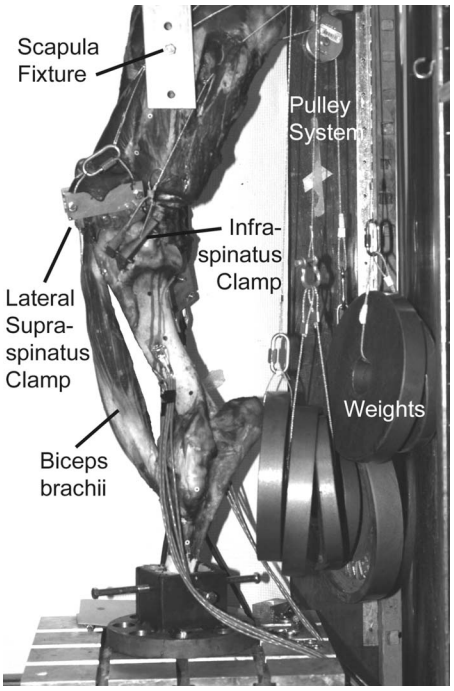

Fig. 1 Lateral view of a simplified preparation of a left equine forelimb in the materials testing machine. The subscapularis (not visible due to its medial origin and insertion sites), infraspinatus, and the lateral and medial head of the supraspinatus were clamped and weighted to simulate active force production as predicted with optimization. The biceps brachii muscle was left intact. Flexion of the elbow joint was due to the rotation of the humerus in relation to the fixed radius and ulna.

experimentally measure strains at the specific bone graft donor and stress fracture sites, strain gauges were applied to locations on the stress fracture cross section except at the lateral aspect where gauges were applied to the bone graft donor site. Before application, each strain gauge location was manually scraped of soft tissue using a scalpel, abraded using a fine-grit sand paper, and degreased with ethanol. Each location was further conditioned and neutralized (M-prep Conditioner A and M-prep Neutralizer SA, Measurements Group Inc., Raleigh, NC). Stacked rectangular triple rosette strain gauges (WK-06-060WR-350, Measurements Group Inc., Raleigh, NC) were individually coated with polyurethane (M-coat A, Measurements Group Inc., Raleigh, NC), bonded to each location using cyanoacrylate adhesive (M-bond 200, Measurements Group Inc., Raleigh, NC), and covered with a silicone adhesive (Devcon) for increased moisture resistance. The middle gauge of each rosette was aligned with the longitudinal axis of the humerus. The longitudinal axis was defined as running from the proximal aspect of the major tubercle to the distal aspect of the lateral epicondyle and the midpoint of this line was used to define the mid-diaphysis of the humerus (Fig. 2). The strain gauge applied to the medial mid-diaphyseal aspect was attached just distal to the muscular attachment site of the teres major and the latissimus dorsi muscles; the two strain gauges applied on the cranial aspect of the humerus were aligned with the intermediate ridge of the bone; the strain gauge applied to the stress fracture location on the neck of the caudal aspect of the humerus was positioned 2 cm distal to the caudal edge of the humeral head (Fig. 3).

Each strain gauge was wired to a Wheatstone bridge circuit, which included a corresponding dummy gauge attached to a second nonloaded humerus for temperature compensation. Strain signals were amplified using data acquisition modules SCXI 1520 or SCXI 1121 (National Instruments Inc., Austin, TX), sampled at

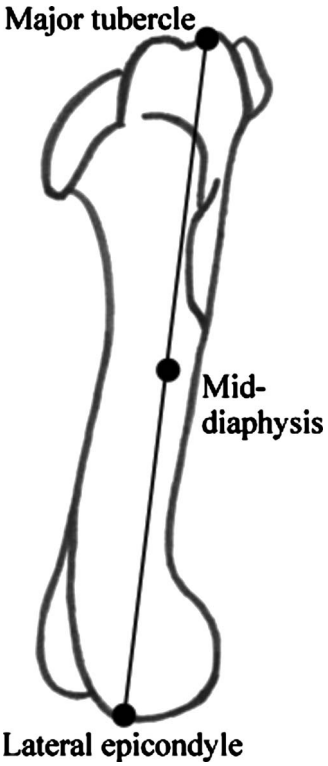

Fig. 2 The longitudinal axis along the lateral aspect of the equine humerus was defined as running from the proximal aspect of the major tubercle to the distal aspect of the lateral epicondyle. The midpoint of this line was used to define the mid-diaphysis of the humerus and the middle gauge of each rosette strain gauge was aligned with the longitudinal axis of the humerus.

500 Hz, and stored using LABVIEW 7.1 (National Instruments Inc., Austin, TX). The gauges were supplied with a constant internal voltage of 5 V (SCXI 1520) or 3.3 V (SCXI 1121). To assure that the same peak forces and strain magnitudes were consistently acquired during a test, each test was performed for 30 cycles of

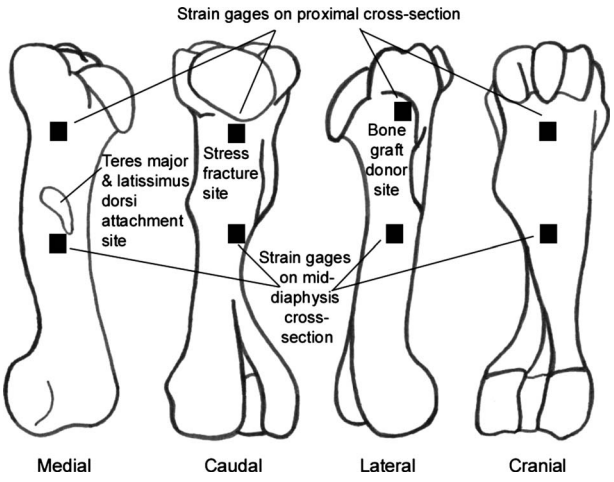

Fig. 3 Right humerus with locations of applied strain gauges at the mid-diaphysis and the proximal cross sections including the specific stress fracture and bone graft donor sites. The gauge located on the medial mid-diaphysis was positioned just distal to the muscular attachment of the teres major and the latissimus dorsi muscles.

force-controlled loading in the materials testing machine from a near zero load to 1600 N at 0.25 Hz. Force data were recorded at 100 Hz using MTS TESTWARE (MTS Systems Corp., Minneapolis, MN). Before principal strains were calculated with the acquired strain data, the raw strain data were reduced. Base line strain data were obtained from the attached strain gauges while the simplified musculoskeletal preparation was positioned in the materials testing machine at a zero-load setting before testing began, and these values were subtracted from all subsequent strain readings. Strain gauges were visually inspected following each test to ensure that bony adhesion was maintained throughout all trials. In addition, strain data obtained from two concurrent tests not presented in this paper confirmed no deviation from base line strain values. Strain data were then identified at a standing vertical ground reaction load of 1335 N and averaged during cycles 20–25. The maximum and minimum principal strain magnitudes and directions for each strain gauge site were then calculated.

For principal strain,

$$\varepsilon_{P,Q} = \frac{\varepsilon_1 + \varepsilon_3}{2} \pm \frac{1}{\sqrt{2}}\sqrt{(\varepsilon_1 - \varepsilon_2)^2 + (\varepsilon_2 - \varepsilon_3)^2} \tag{1}$$

For principal angle measured from principal axis to Grid 1,

$$\theta = \frac{1}{2}\tan^{-1}\left(\frac{\varepsilon_1 - 2\varepsilon_2 + \varepsilon_3}{\varepsilon_1 - \varepsilon_3}\right) \tag{2}$$

For principal angle measured from grid 1 to principal axis,

$$\phi_{P,Q} = -\theta \tag{3}$$

subject to the following rules:

(a) if $\varepsilon_1 > \varepsilon_3$, then $\phi_{P,Q} = \phi_P$
(b) if $\varepsilon_1 < \varepsilon_3$, then $\phi_{P,Q} = \phi_Q$
(c) if $\varepsilon_1 = \varepsilon_3$ and $\varepsilon_2 < \varepsilon_1$, then $\phi_{P,Q} = \phi_P = -45$ deg
(d) if $\varepsilon_1 = \varepsilon_3$ and $\varepsilon_2 > \varepsilon_1$, then $\phi_{P,Q} = \phi_P = +45$ deg
(e) if $\varepsilon_1 = \varepsilon_2 = \varepsilon_3$, then $\phi_{P,Q}$ is indeterminate (equal biaxial strain)

In the equations above, ε_P is the maximum principal strain, ε_Q is the minimum principal strain, ε_1, ε_2, ε_3 are the strains from the three grids of the rosette labeled in counterclockwise order, $\phi_{P,Q}$ is the principal angle calculated as the angle from Grid 1 to a principal axis, and ϕ_P and ϕ_Q represent the principal angles referenced to Grid 1 corresponding to ε_P and ε_Q, respectively (Fig. 4). To reference principal strain directions to the longitudinal axis of the humerus, principal strain directions were also calculated as the angle from Grid 2 to a principal axis by adding 45 deg to and subtracting 45 deg from $\phi_{P,Q}$.

Maximum and minimum principal stresses, σ_P and σ_Q, respectively, were calculated at each rosette for an isotropic homogeneous material:

$$\sigma_P = \frac{E}{1 - \nu^2}(\varepsilon_P + \nu\varepsilon_Q) \tag{4}$$

$$\sigma_Q = \frac{E}{1 - \nu^2}(\varepsilon_Q + \nu\varepsilon_P) \tag{5}$$

where E is the elastic modulus=18 GPa, and ν is Poisson's ratio =0.3 for cortical bone [7]. At each strain gauge location, shear strain was also calculated in the local humeral coordinate system, where the x axis was defined distal to proximal on the longitudinal axis of the bone, the y axis was caudal to cranial, and the z axis was lateral to medial. Shear strains were calculated in the x-y plane for medial and lateral strain gauge locations, and in the x-z plane for caudal and cranial locations.

The mean, standard deviation, median, and range were calculated for all variables including the strains from each grid of the rosette, the maximum and minimum principal strains and directions, the maximum and minimum principal stresses, and the

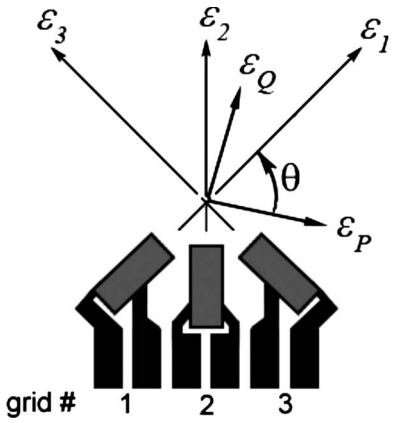

Fig. 4 The three grids of the triple rosette strain gauge labeled in the counterclockwise direction produce the three strains ε_1, ε_2, and ε_3, which were used to calculate the principal strains and corresponding directions. ε_P and ε_Q are the maximum and minimum principal strains respectively. θ represents the principal angle measured from the axis of maximum principal strain to Grid 1. Note the axis of Grid 2 points along the longitudinal axis of the humerus.

shear strains for the eight specimens.

Strains from Grid 2 of each triple rosette strain gauge, which was aligned with the longitudinal axis of the humerus, were averaged at each strain gauge location and compared to the calculated magnitudes and directions of the corresponding mean principal strains. Of the maximum and minimum principal strain values calculated at each location, the minimum principal strains occurred in the direction closest to the longitudinal axis of the bone and were therefore used for all comparative analyses. A paired t-test with a significance level of $p \leq 0.05$ was used to compare the longitudinal and principal strain magnitudes, and the direction of principal strain was analyzed.

In cases where the longitudinal and principal strains were comparable, the validity of the mathematical model was then tested. The predicted strains from the mathematical model were compared to experimentally determined longitudinal strains at each location on the humerus by assessing box plots of the data. Predicted strains were considered comparable if they occurred within ± 2 standard deviations from the mean longitudinal strain.

Due to the technical problems, not all analyses could be completed with the full number of specimens. Therefore, $n=8$ for all strain gauge locations with all of the muscles weighted to active force, except for the proximolateral aspect of the humerus where $n=6$.

Results

At the middle of the diaphysis of the humerus, the minimum principal strains were not significantly different from longitudinal strains from Grid 2 at the caudal aspect ($p=0.1237$), and the principal strain direction was 16 deg (Table 1). Strains at the cranial aspect were significantly different ($p<0.0001$) with tensile longitudinal strains, compressive minimum principal strains, and a principal strain direction of −18 deg. At the lateral aspect, longitudinal and principal strain magnitudes were significantly different ($p=0.0065$) but comparable in magnitude (less than 9% difference referenced to the principal strain), and the principal strain direction was −11 deg. At the medial aspect, compressive minimum principal strains of a higher magnitude than the longitudinal strains were calculated, so that the strains were significantly different and not comparable ($p=0.0034$), though the principal strain direction was small (2 deg). As a result, only the strains at the caudal and lateral aspects of the middle of the diaphysis were further analyzed.

At the proximal humerus, the longitudinal and principal strains at the caudal aspect (stress fracture site) were significantly different ($p=0.0437$) (Table 1), yet the strains were comparable (7% difference referenced to the principal strain) and the principal strain direction was small (2 deg). Both longitudinal and principal strains at the cranial and medial aspects of the humerus fell within a $\pm 20\mu\varepsilon$ range and were considered negligible. At the bone graft

Table 1 Comparison of average longitudinal strains from Grid 2 of each rosette strain gauge and average principal strains at the caudal, cranial, lateral, and medial aspects of the middle of the diaphysis and proximal humerus. The caudal and lateral aspects of the proximal humerus represent the specific stress fracture site and the specific bone graft donor site, respectively. A *p* value ≤0.05 implies a significant difference between the longitudinal and principal strain means. Positive principal strain direction was measured clockwise from the longitudinal axis of the humerus. Predicted strain magnitudes are from the mathematical model presented in Part I of this two-part article. Compressive values are negative and tensile values are positive.

		Average longitudinal strain (Grid 2) ($\mu\varepsilon$)	Average minimum principal strain magnitude ($\mu\varepsilon$)	p value (from paired t-test)	Average minimum principal strain direction (deg)	Shear strain ($\mu\varepsilon$)	Predicted strain magnitudes from math model ($\mu\varepsilon$)
Middle of the diaphysis	Caudal	−242	−427	0.1237	16	118	−377
	Cranial	111	−81	<0.0001[a]	−18	25	258
	Lateral	−127	−139	0.0065[a]	−11	27	−169
	Medial	−194	−280	0.0034[a]	2	10	107
Proximal cross-section	Caudal (stress fracture site)	−68	−73	0.0437[a]	2	3	−35
	Cranial	18[b]	−7[b]	<0.0001[a]	27	3	−65
	Lateral (bone graft donor site)	−287	−339	0.0253[a]	6	35	−53
	Medial	1[b]	−7[b]	0.0424[a]	−2	0	−16[b]

[a] p value ≤0.05.
[b] Strain values within a $\pm 20\mu\varepsilon$ range considered negligible.

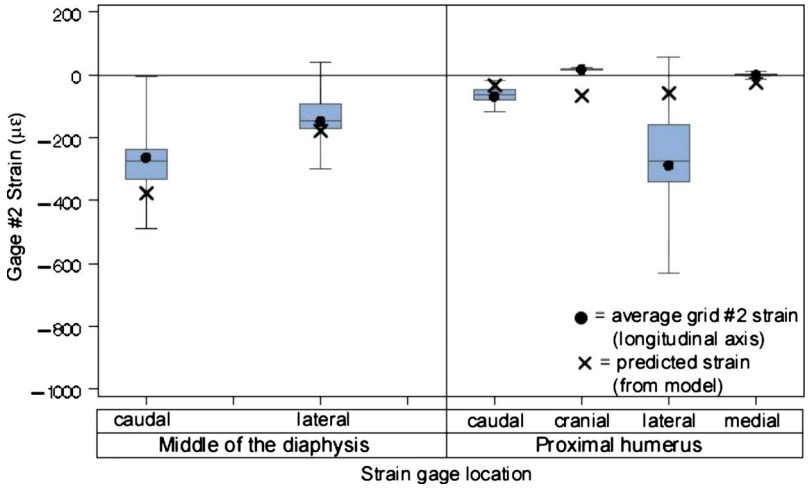

Fig. 5 Comparison of the distribution of longitudinal strains (from Grid 2) with the predicted strains from the mathematical model formulated in Part I of this two-part article at the middle of the diaphysis and the proximal humerus. The caudal and lateral aspects of the proximal humerus represent the stress fracture and bone graft donor sites, respectively. The top and bottom lines of each box represent the 75th and 25th percentile of data, respectively, the middle line represents the median, and the outlying lines represent ±2 standard deviations from the mean. Compressive values are negative and tensile values are positive.

donor site (lateral aspect), the longitudinal and principal strains were larger in magnitude and statistically different ($p=0.0253$), but comparable in magnitude (15% difference referenced to the principal strain), and the principal strain direction was 6 deg. The strains at the caudal and lateral aspects were further analyzed because they were comparable and the strains at the cranial and medial aspects were further analyzed due to their negligible values.

When comparing the experimentally measured strains in the longitudinal direction with the predicted strain from the mathematical model at the middle of the diaphysis, the predicted strains were compressive at both the caudal and lateral aspects and were within ± 2 standard deviations of the mean longitudinal strain (Fig. 5). At the proximal humerus, the predicted strains at the caudal and lateral aspects were compressive and were within ± 2 standard deviations of the mean longitudinal strain (Fig. 5). At the cranial aspect, the predicted strain was compressive whereas the longitudinal strain was tensile. However, the predicted strain value was small ($-65\mu\varepsilon$) and longitudinal strain was negligible (within a $\pm 20\mu\varepsilon$ range). At the medial aspect, both the mean longitudinal strain and predicted strain were negligible ($1\mu\varepsilon$ and $-16\mu\varepsilon$, respectively).

Discussion

The goal of this study was to experimentally validate the musculoskeletal model of the equine forelimb presented in Part I by directly measuring strains at the donor site for bone grafts, the site predisposed to stress fracture, the medial and cranial aspects of the transverse cross section corresponding to the stress fracture site, and the middle of the diaphysis of the humerus of a simplified in vitro laboratory preparation. The first objective was to determine surface bone strain magnitudes and directions at all strain gauge locations. The second objective was to determine whether computing strains solely in the direction of the longitudinal axis of the humerus in the mathematical model was inherently limited by comparing the experimental strain readings from the middle grid of each strain gauge rosette (also aligned with the longitudinal axis of the bone) to the principal strain magnitudes and directions. The final objective was to determine whether the mathematical model formulated in Part I was valid for determining the bone surface strains at the various locations on the humerus where experimentally measured longitudinal strains correlate to principal strains. Key results are that the strains in the direction of the longitudinal axis of the humerus were not comparable to the principal strains at the cranial and medial aspects of the middle of the diaphysis but were comparable to the principal strains at the caudal and lateral aspects of the middle of the diaphysis and at all aspects of the proximal humerus. Further analysis of the six locations where longitudinal and principal strains were comparable indicated that the mathematical model formulated in Part I predicts strains at all six locations that compare favorably with experimentally measured strains.

The simplified laboratory preparation of the equine humerus on which to apply strain gauges involved a number of assumptions. First, mechanically loading the simplified preparation at one location on the scapula while allowing flexion of the shoulder and elbow joints was assumed to closely mimic in vivo loading conditions. In the horse, the long column of equine forelimb bones is supported by the attachment of the extrinsic serratus ventralis muscle to the medial aspect of the scapula [9], and in vitro loads were applied at a point on the scapular spine between the distal portions of the two triangular areas of insertion of the serratus ventralis muscle. Second, although the biceps brachii muscle spans both the shoulder and elbow joints and neither originates nor inserts directly on the humerus, including the biceps brachii muscle-tendon complex was assumed to be necessary because the contact force created by this muscle on the proximocranial aspect of the humerus contributes to the structural integrity of the column of forelimb bones by preventing flexion of the shoulder joint [9,10]. Third, exclusion of all shoulder muscles that were not predicted to be active while the horse is standing was assumed valid for the purpose of identifying a simplified preparation. Although the presence and locations of inactive muscles may provide passive forces that influence strains of the humerus, their contribution to humeral strains was considered negligible in comparison with that of the active muscles. Finally, analyzing strains at 1335 N load of a cyclically loaded specimen was assumed to be indicative of strains while the horse is standing.

Although some of the results from the paired t-test used to compare the longitudinal and minimum principal strains indicated that the difference between the strain values was statistically significant (lateral aspect at the middle of the diaphysis and caudal and lateral aspects of proximal cross section, Table 1), the small percent difference between the strain magnitudes (range of 7–15%) indicated that the difference was not practically important. At all of these locations, the longitudinal and minimum principal strains were considered comparable.

Comparing experimentally measured longitudinal strains with corresponding minimum principal strain magnitudes and directions determined whether modeling strains solely in the direction of the longitudinal axis of the humerus in Part I was a valid assumption. The longitudinal and principal strains were not comparable at the cranial and medial aspects of the middle of the diaphysis of the humerus; thus the mathematical model, and possibly the assumptions used to formulate the model, was considered insufficient. Neglecting the contributions of the shear force and torsional moment to the stresses in the mathematical model may have influenced the predicted strains at these locations. However, the shear strains calculated from strain gauge data at the cranial and medial aspects of the middle of the diaphysis were small ($25\mu\varepsilon$ and $10\mu\varepsilon$, respectively) (Table 1). Accordingly, this experimental result supports neglecting the shear force and torsional moment in the model.

Another possible source of error might be the loads applied to the bone. The bending moment values required to develop the experimental strains at the cranial and medial aspects of the middle of the diaphysis are $M_y=-42.2$ N m in the sagittal plane and $M_z=20.2$ N m in the cranial plane (as opposed to the previously calculated values of −6.8 N m and 71.3 N m, respectively). Predicted strains at the caudal and lateral aspects according to these moment values are still within ± 2 standard deviations of the experimental mean longitudinal strain. Either greater magnitude shoulder muscle forces or a lesser magnitude scapula contact load are necessary to yield bending moment values that correspond to experimental strains. Alternatively, the muscles assumed to be inactive during standing might actually contribute substantial forces and moments to this region of the bone. Therefore, the optimized loads due to the shoulder muscles and contacts on the humerus may not completely depict the loads experienced at middle of the diaphysis while the horse is standing. Thus neglecting the shoulder muscles that were assumed to be inactive may be the cause of discrepancy between calculated and measured strains at these locations.

Comparing the predicted strains with experimentally measured longitudinal strains at the six locations where the minimum principal strains were comparable tested the validity of the mathematical model. The direct comparison revealed that the predicted strains were either within ± 2 standard deviations of the measured strains (four of six locations) or the predicted and measured strains were negligible (two of six locations). Because the mathematical model was validated for predicting strains at these six locations, the assumptions used to formulate the model may also be validated for determining strains at these locations. This leads to the presumption that these locations at the middle of the diaphysis and proximal humerus are not highly affected by torsional loads; the assumed homogeneity, isotropy, and other material properties of the cortical bone are suitable; the muscles assumed to be inactive during standing did not contribute substantial forces and moments to the proximal region of the bone.

The compressive longitudinal strain of $-287\mu\varepsilon$ found at the site proposed for harvest of autogenous bone graft material indicates that this region experiences compressive strains while the horse is standing. Introducing a 12 mm diameter hole in the cortical bone at this location to obtain the internal bone graft material has been proposed [3]. Given that the lateral aspect of the proximal humerus is approximately 75 mm in width, the theoretical stress concentration factor from introducing such a hole is 2.5. Thus strains in this region would approach $-700\mu\varepsilon$. Considering that compressive strains as high as $-2600\mu\varepsilon$ have been measured in vivo on the radius while the horse is pacing [2], the strain experienced at the proximolateral aspect of the humerus with the introduction of the 12 mm diameter hole is relatively low and thus should not adversely affect the structural integrity of the bone while the horse is standing.

The results from the mathematical model in conjunction with the experimentally determined strains at the two of eight locations where the model was inaccurate are useful toward several purposes. Knowing that the act of standing does not produce significant strains in the proximal aspect of the equine humerus implies that standing alone does not inflict significant strains to the proximocaudal aspect of the equine humerus and thus is not the cause of stress fractures. The finding of a longitudinal compressive strain of approximately $-300\mu\varepsilon$ at the site of the humerus proposed for harvest of autogenous bone graft material indicates that this region of the humerus is not adversely affected by the introduction of a hole necessary to obtain the donor bone graft material while the horse is standing. The strains associated with recovery from anesthesia are unknown, however. The experimental results at the middle of the diaphysis indicate tensile longitudinal strains at the cranial aspect and compressive strains at the caudal aspect, which are useful in determining the placement of internal fixation devices for stabilizing fractures in this region of the humerus [2].

In summary, the measured strains in the longitudinal direction were not comparable to the principal strains at the cranial and medial aspects of the middle of the diaphysis of the equine humerus. Accordingly the mathematical model formulated in Part I was inherently limited in computing strains solely in the longitudinal direction of the humerus at these two locations. At the remaining six locations where the longitudinal and principal strains were comparable, however, the mathematical model predicted strains at all six locations that compare favorably with experimentally measured strains. Therefore, the mathematical model is useful for predicting strains at the caudal and lateral aspects of the middle of the diaphysis and all four aspects of the proximal humerus while the horse is standing.

Acknowledgment

Funding was provided by a grant from the Center for Equine Health at the University of California, Davis. The authors would also like to thank Tanya Garcia-Nolan and Ken Taylor for contributions to this work.

References

[1] Pollock, S., Hull, M. L., Stover, S. M., and Galuppo, L. D., 2008, "A Musculoskeletal Model of the Equine Forelimb for Determining Surface Stresses and Strains in the Humerus—Part I. Mathematical Modeling," ASME J. Biomech. Eng., **130**(4), p. 041006.

[2] Turner, A. S., Mills, E. J., and Gabel, A. A., 1975, "In Vivo Measurement of Bone Strain in the Horse," Am. J. Vet. Res., **36**(11), pp. 1573–1579.

[3] Harriss, F. K., Galuppo, L. D., Decock, H. E., McDuffee, L. A., and Macdonald, M. H., 2004, "Evaluation of a Technique for Collection of Cancellous Bone Graft From the Proximal Humerus in Horses," Vet. Surg., **33**(3), pp. 293–300.

[4] Korsgaard, E., 1982, "Muskelfunktionen I Hestens Forben, En Elektromyografisk Og Kinesiologisk Undersogelse," Ph.D. thesis, De. Kgl. Veterinaer—og Landbohojskole, Institut for Kirurgi, Kobenhavn, Denmark.

[5] Tokuriki, M., 1973, "Electromyographic and Joint-Mechanical Studies in Quadrupedal Locomotion. I. Walk," Nippon Juigaku Zasshi, **35**(5), pp. 433–436.

[6] Crowninshield, R. D., and Brand, R. A., 1981, "A Physiologically Based Criterion of Muscle Force Prediction in Locomotion," J. Biomech., **14**(11), pp. 793–801.

[7] Gross, T. S., McLeod, K. J., and Rubin, C. T., 1992, "Characterizing Bone Strain Distributions in Vivo Using Three Triple Rosette Strain Gages," J. Biomech., **25**(9), pp. 1081–1087.

[8] Rybicki, E. F., Simonen, F. A., and Weis, E. B., Jr., 1972, "On the Mathematical Analysis of Stress in the Human Femur," J. Biomech., **5**(2), pp. 203–215.

[9] Dyce, K. M., Sack, W. O., and Wensing, C. J. G., 2002, *Textbook of Veterinary Anatomy*, 3rd ed., Elsevier Science, Philadelphia, PA, pp. 568–605.

[10] Nevens, A. L., Stover, S. M., and Hawkins, D. A., 2005, "Evaluation of the Passive Function of the Biceps Brachii Muscle-Tendon Unit in Limitation of Shoulder and Elbow Joint Ranges of Motion in Horses," Am. J. Vet. Res., **66**(3), pp. 391–400.